Design and Evaluation of Microphone Cavity Geometries for Wind-Tunnel Acoustic Measurements

van Dercreek, Colin; Manjunath, Pranav; Ragni, Daniele; Snellen, Mirjam

DOI
10.2514/6.2019-1580

Publication date
2019

Document Version
Final published version

Published in
AIAA Scitech 2019 Forum

AIAA SciTech Forum
7-11 January 2019, San Diego, California
AIAA Scitech 2019 Forum

10.2514/6.2019-1580

Design and Evaluation of Microphone Cavity Geometries for Wind-Tunnel Acoustic Measurements

Colin P VanDercreek*, Pranav Manjunath†, Daniele Ragni‡ and Mirjam Snellen§
Delft University of Technology, 2629HS Delft, Netherlands

This study investigated how embedding microphones in different cavity geometries reduce the measured turbulent boundary layer pressure fluctuations at the microphones. The cavity geometries were systematically varied using a design of experiments (DOE) methodology. This approach tested different cavity depths, diameters, chamfers, and opening sizes as well as the effect of a fine mesh covering. The resulting wind-tunnel test data was analyzed using a generalized additive statistical model (GAM). This approach quantified the relative effect of these parameters on the response variables of interest while accounting for non-linear frequency dependence. This experimental investigation showed that a mesh reduces the boundary layer noise by 8 dB. It was also shown that reducing the cavity area from the wall to the base of the microphone reduces the measured boundary layer spectral energy. Additionally, the model quantified the complex interactions between the mesh and area as well as the change in area.

I. Nomenclature

$\boldsymbol{b}$	=	Random effects coefficient vector
d	=	Cavity depth
E_r	=	Measured hot-wire voltage
$E_{w,r}$	=	Temperature corrected hot-wire voltage
k	=	Wavenumber
M	=	Mach number
m	=	Number of model terms
n	=	Number of observations
p	=	Number of random model terms
R	=	Dimensionless acoustic resistance of mesh
H	=	Boundary layer shape factor
T_r	=	Hot-wire reference temperature
T_w	=	Hot-wire temperature
T_a	=	Tunnel ambient temperature
U_∞	=	Tunnel free stream velocity
u^+	=	Dimensionless boundary layer velocity
u^*	=	Friction velocity
$\boldsymbol{X}$	=	Design matrix of model terms
$\boldsymbol{y}$	=	Vector of model response variable
y^+	=	Dimensionless height above the wall
$\boldsymbol{Z}$	=	Design matrix of random effects terms
$\boldsymbol{\alpha}$	=	Level of statistical significance
$\boldsymbol{\beta}$	=	Linear regression coefficients vector
δ	=	Boundary layer thickness at $0.99U$
$\boldsymbol{\epsilon}$	=	Linear regression error vector

*Ph.D. Candidate, Aircraft Noise and Climate Effects (ANCE),Section, Faculty of Aerospace Engineering, Kluyverweg 1, c.p.vandercreek-1@tudelft.nl, Member AIAA
†Ph.D. Candidate, Aircraft Noise and Climate Effects (ANCE),Section, Faculty of Aerospace Engineering, Kluyverweg 1, P.Manjunath@tudelft.nl
‡Assistant Professor, Aerodynamics, Wind Energy, Flight Performance and Propulsion (AWEP), Department, Faculty of Aerospace Engineering, Kluyverweg 1, D.Ragni@tudelft.nl, Member AIAA
§Associate Professor, Aircraft Noise and Climate Effects (ANCE) Section, Faculty of Aerospace Engineering, Kluyverweg 1, M.Snellen@tudelft.nl

Φ_{pp} = Power spectral density
τ_w = Wall shear stress
ν = kinematic viscosity

II. Introduction

Turbulent boundary layer (TBL) noise generated by the wind tunnel wall along with other acoustic noise sources limit acoustic measurements in closed wind tunnels. Typically use is made of acoustic arrays for aeroacoustic measurements. One way of countering the disturbing effect of TBL fluctuations on the measurements is to use beamforming with diagonal removal [1, 2]. This noise is primarily due to the non-linear interaction between turbulent eddies inside the boundary layer [3] as well as the pressure fluctuations in the viscous and logarithmic regions of the boundary layer [4]. A complementary approach to improving acoustic measurements is by recessing microphones in cavities [5]. The focus of this study is to evaluate how cavity geometries influence the impingement of boundary layer pressure fluctuations on a microphone. This creates a lower limit below which acoustic measurements are not feasible due to the acoustic levels generated by the test article overwhelmed by this background noise [5].

Acoustic arrays are often used in conjunction with beamforming algorithms to localize and quantify acoustic noise within a region of interest. Typical sound levels for a conventional airfoil are around 60 dB m^{-1} depending on the flow conditions [6]. As the sound generation characteristics of airfoils improve by incorporating features such as trailing edge serrations [7] to reduce noise, it is important to improve acoustic measurement techniques. One of the ways to counter the disturbing effect of TBL fluctuations on the measurements is to use beamforming with diagonal removal. Doing so, reduces the effect of TBL noise by taking advantage of the incoherent nature of this source [8]. This can reduce the measured background noise by approximately 25 dB at 5 kHz for a tunnel Mach number of 0.22 [5]. However, it is advantageous to couple these signal processing techniques with actual reductions in the TBL fluctuations. A common approach to reducing TBL wall noise is by recessing the microphones in cavities and covering these cavities with a metallic mesh or Kevlar [5, 9, 10]. These approaches, coupled with array processing, can approximately reduce the measured background noise by an additional 10 dB for an array [5]. This results in a typical improvement in signal-to-noise ratio (SNR) by 5 dB.

Increasing the cavity depth reduces the wall pressure fluctuations measured by the microphones by increasing the distance from the local boundary layer [10]. The mesh also reduces these fluctuations while attenuating high frequency noise. The physical explanation for the reduction in pressure can be seen in the equations for wave propagation from duct acoustics [11] which solve the wave equation in an infinite duct. Equation 1 is the generalized solution for the pressure distribution within a cylindrical duct, where z is distance along the propagation path from the source, r is the radial position, θ is the angular position, $k_{m\mu}$ is the axial wave number, $A_{m\mu}$ is the downstream propagating coefficient, $B_{m\mu}$ is the upstream propagating coefficient, and $U_{m\mu}$ is the radial coefficient, m and μ are the modes.

$$P(z, r, \theta) = \sum_{m=\infty}^{\infty} \sum_{\mu=1}^{\infty} \left(A_{m\mu} e^{ik_{m\mu}z} + B_{m\mu} e^{-ik_{m\mu}z} \right) U_{m\mu}(r) e^{-im\theta} \tag{1}$$

The relevant portion of eq. 1 is the expression $e^{-ik_{m\mu}z}$. When the axial wave number is imaginary, the energy dissipates exponentially. Equation 2 is the expression for the axial wave number, where ω is the angular frequency and $\alpha_{m\mu}$ is the radial wave number.

$$k_{m\mu} = \sqrt{\omega^2 - \alpha_{m\mu}} \tag{2}$$

The radial wave number are the solutions to the first derivative of a Bessel function of the first kind and is proportional to the duct diameter [11]. When $k_{m\mu}$ is imaginary, the mode is cut-off. In practice, for the cavity diameters of interest in this study, 1 cm, all modes but the planar mode are cut-off which results in the TBL pressure fluctuations decaying with depth. Equation 3 describes the reduction in the measured turbulent boundary layer noise due to the presence of a mesh, where R is the dimensionless acoustic resistance of the mesh *.

$$\Delta SPL_{mesh} = -10log10 \left[1 + \frac{R^2}{4} \left(\frac{1}{(0.7M)^2} - 1) \right) \right] \tag{3}$$

An experiment was conducted to further study the influence of cavity geometry on two response variables: the contribution of pressure spectral energy due to the boundary layer. The long term application of this experimental data

* Sijtsma, personal communication, March 14, 2018

and model is to support future deterministic model development with the long-term goal of optimizing cavity designs. This experiment used a design of experiments (DOE) methodology. DOE is a statistical tool for test planning, that ensures randomization while covering a wide range of the design space of interest. The primary advantage of DOE over the more traditional one factor at a time approach to testing is that it reduces required test resources by making more efficient use of the potential experimental design space while providing insight into how different factors interact with each other [12]. The resulting test matrix ensures a sufficient number of runs to quantify the influence of different factors with statistical confidence. The resulting data were then used to develop a stochastic model which is useful for extracting which parameters have the most influence on the response variables.

In this experiment the following geometric parameters were systematically varied: depth, diameter, mesh, chamfer, and cavity opening percentage. The wind tunnel speed was varied to determine if different designs perform better at different wind speeds. A generalized additive model (GAM) with mixed effects was developed to quantify the relationship between different geometries and the boundary layer energy response variable. This approach was able to determine which cavity geometries influenced the amount of turbulent boundary layer spectral energy.

III. Experimental Set-up

The focus of this experimental campaign was to evaluate the effect of different cavity geometries on the boundary layer spectral energy at the microphone location. In addition to the pressure measurements, the boundary layer was evaluated with hot-wire anemometry (HWA). HWA data were used to calculate boundary layer thickness (δ), the shape factor (H), and to estimate the friction velocity (u^*). These properties are required to normalize the pressure spectra of the boundary layer[4, 13].

A. Experimental Design

An experimental design methodology was used to efficiently characterize the main effects of the different geometric parameters on the level of TBL spectral energy with statistical confidence. This methodology is widely used in many research fields as well as industrial applications [14, 15]. For this experiment, DOE was used to design a test campaign to analyze the boundary layer energy response variables. Based on previous experiments [5, 9, 10], cavity depth, diameter, chamfer, percent of gap, mesh covering, and tunnel velocity were selected as test factors to evaluate the spectral energy. A D-optimal[14] design criterion was used to optimize the design to fit the resulting data to a generalized additive model. This criterion determines how many experimental runs and the random combinations of geometric variables to achieve statistical power of greater than 0.95. Statistical power is the probability that the experiment will result in statistically significant result for each factor. The significance level, α was chosen to be 0.05. A D-optimal design minimizes the correlation between test factors (the cavity geometric parameters) by maximizing the difference between the values of each factor for each run which is ideal for quantifying the potential design space [14]. For this experiment, the test factors, their range of values, and statistical power are listed in table 1.

This DOE was performed using the *R* software package, *skpr* [16]. The resulting design consists of 12 randomized cavity geometries that were tested 12 times at two different velocities for a total of 144 random runs. The levels for these factors and their estimated power is shown in table 1. Figure 1 is the correlation matrix between all of the factors. As shown by this figure, the correlation between factors is low, which means there were a sufficient number of runs to fully evaluate the design space without conflating the effect of two or more factors [14]. Measurements were made at 12 randomized run conditions, which includes 3 replications at different tunnel speeds. However, to avoid the complexity of swapping cavities randomly over 144 runs, it was decided to design two different plates, each with 6 cavities and a flush mounted microphone. The run order of these two plates was randomized. In order to cover the same design space by adjusting the more conventional one factor at a time (OFAT) approach, would require 1458 different runs [12], which doesn't include any beneficial replications.

B. Cavity Test Article Design

When designing the plate to ensure statistical independence of the measurements, each cavity was spaced 120 mm apart to avoid span-wise coherence [17, 18]. Table 2 lists the randomized cavity designs and their corresponding geometric parameters. Figure 2 illustrates the definition of these parameters. A stainless steel mesh was installed with epoxy. The mesh has a density of 200 threads per cm with a wire diameter of 0.025 mm. In addition to the cavities, a flush mounted microphone was mounted on each plate as a baseline measurement. For additional comparison, a GRAS 40LS surface mount microphone was also used which has a dynamic range of 121 dB with an error of ±1 dB up to

Table 1 Experimentally Varied Factors

Factor	Type	Levels	Estimated Power
Tunnel Speed, m/sec	Continuous	30.0, 70.0	0.99
Diameter, mm	Continuous	5.0, 10.0	0.99
Mesh	Categorical	Yes, No	0.99
Depth, mm	Continuous	0.0, 5.0, 10.0	0.99
Gap, %	Continuous	50, 100	0.99
Chamfermm	Continuous	0.0, 4.0	0.99

Table 2 Cavity Geometries

Designation	Diameter (mm)	Mesh	Depth (mm)	Gap	Chamfer (mm)
1A	10.0	Yes	5.0	100	4.0
2A	10.0	Yes	10.0	100	0.0
3A	5.0	No	5.0	100	4.0
4A	5.0	No	5.0	50	0.0
5A	10.0	Yes	10.0	50	4.0
6A	10.0	No	5.0	100	0.0
Flush A	6.0	No	0.1	100	0.0
7B	5.0	No	10.0	50	0.0
8B	5.0	Yes	10.0	100	0.0
9B	10.0	No	10.0	50	0.0
10B	5.0	Yes	5.0	100	4.0
11B	10.0	Yes	10.0	50	4.0
12B	5.0	No	5.0	50	4.0
Flush B	2.7	No	1.0	100	0.0
40LS	6.35	No	-2.5	100	0.0

20 kHz.

C. Experiment Details

The experiment was conducted at the TU Delft Low Turbulence Tunnel (LTT). The LTT is an atmospheric closed test section wind tunnel capable of airspeeds up to 120 m/sec. The test section is 1.8 m wide by 1.25 m tall. Free-stream turbulence is 0.015% with smooth walls. The tunnel has a contraction ratio of 17.8. The cavity plates were flush mounted to the bottom of the test section. 24 runs were performed with the plates, the presence of the acoustic support, and velocity randomized within these 24 runs. For the runs without an acoustic source, the entire speaker support was removed from the tunnel to minimize noise sources other than the empty tunnel. Data were also collected at 50 m/sec for all runs.

D. Data Acquisition

Pressure measurements were made with a combination of LinearX M51 and M53 $\frac{1}{2}$" condenser microphones with a dynamic range of 122 dB up to 20 kHz with an error of ±1 dB. The microphone baffles were removed and the microphones were directly mounted at the base of each cavity. A National Instruments data acquisition system (DAQ) NI9215 acquired the microphone data at 51 200 Hz. For every run, data for each cavity in the installed plate were captured simultaneously. Forty seconds of data were taken. Between each cavity configuration change, the microphone positions were redistributed randomly to reduce the likelihood of biased data due to microphones having an offset. The microphones were calibrated with a calibrated GRAS 42AA piston phone immediately after completing the acoustic

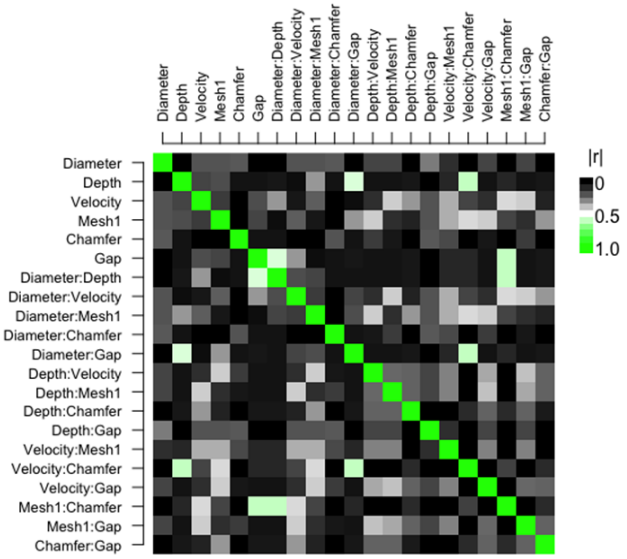

Fig. 1 Correlation matrix of interaction between experimental factors

(a) Gap Illustration **(b) Chamfer, Depth, and Diameter Illustration**

Fig. 2 Illustration of Geometric Parameters

measurements.

E. Hot-Wire Measurements

A calibrated Dantec 1-channel hot-wire probe measured the velocity profile at 9 different span-wise locations. The sample rate was 50 kHz with a 10 kHz low-pass filter with a 3 % measurement uncertainty. Each span-wise measurement point corresponds to a cavity location. The probe was located 25 mm in front of each cavity. The boundary layer was measured at 30 m/sec and 70 m/sec.

IV. Experimental Results

HWA measured the boundary layer properties at 9 positions and two free-stream velocities. The measurements show no variation in boundary layer properties with span-wise position. The mean properties with their 95 % confidence intervals are shown in table 3. These HWA measured the profiles 1.5 m downstream of the tunnel nozzle. Temperature variations in the free-stream flow are the primary source of measurement error due to the variation in tunnel temperature over the long time spent to characterize the boundary layer at each span-wise location. The recorded temperature range during each measurement campaign was used to correct the HWA measurements. Equation 4 was applied to correct the boundary layer measurements [19].

$$E_{w,r} = E_w \sqrt{\frac{T_w - T_r}{T_w - T_a}} \tag{4}$$

The resulting profiles are shown in figure 3a. The boundary layer properties were calculated from the mean of HWA measurements. These properties are listed in table 3. From the shape factor, H, it is evident that the boundary layer for both velocities is fully turbulent.

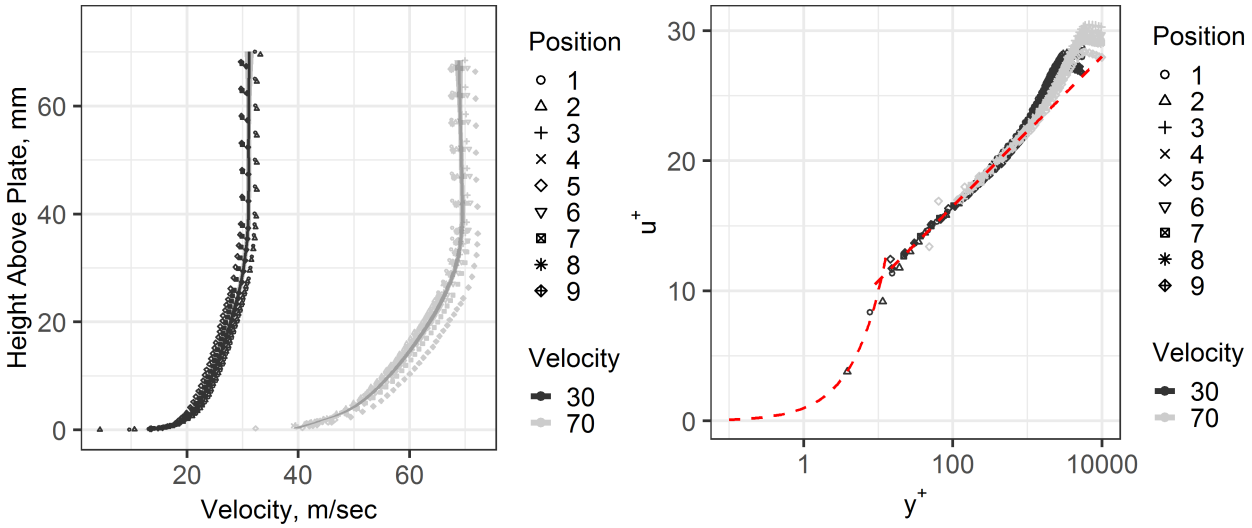

(a) Boundary layer velocity profiles **(b) Boundary layer data logarithmic profile fit**

Fig. 3 Boundary layer data

The friction velocity, u^* was estimated by fitting the boundary layer data to the standard profile for turbulent flat plate boundary layers [20]. This was done by normalizing the boundary layer profile in terms of $u^+ = \frac{u}{u^*}$ and $y^+ = \frac{yu^*}{\nu}$ and fitting the data until a value for u^* minimized the error between the measured data and theory. For this fit it was assumed that the wind tunnel surface was smooth. The value of u^* is listed in table 3. For the 30 m/sec measurements, it was possible to get the HWA probe within 0.5 mm of the wall. For the 70 m/sec case, it was only possible within 2.5 mm due to vibrations in the support sting.

Table 3 Boundary Layer Properties

Velocity (m/sec)	Re	δ (mm)	H	u^* (m/sec)	τ_w (Pa)
30.0	21116	36.5 [32.2, 40.8]	1.32 [1.30,1.33]	1.13 [1.09, 1.16]	1.52 [1.42, 1.62]
70.0	49271	32.5 [30.4, 34.6]	1.28 [1.27,1.29]	2.36 [2.32, 2.40]	6.60 [6.37, 6.83]

A. Microphone Measurements

The performance of the cavities was evaluated between 250 Hz and 7 kHz, the frequencies typically of interest for aeroacoustic research. All analysis used the 30 m/sec and 50 m/sec runs. These runs corresponded with Reynolds numbers of 21,116 and 35,194 based on a 1 cm diameter cavity. Figures 4 and 5 show the influence of cavity design on the measured TBL spectral energy, Φ_{pp}. Spectral energy is normalized by free stream velocity U_∞, wall shear stress τ_w, and the boundary layer thickness, δ. The angular frequency, ω is normalized by the ratio between δ and U_∞. Cavity 6A is not covered with a stainless steel mesh and the cavity area does not change with depth. At the x-axis value of 1, the spectral energy is slightly less than the baseline flush case. Cavity 10B has a mesh and due to the added chamfer, the area decreases with depth. This cavity shows much less TBL spectral energy at the same point as cavity 6A. This shows a clear effect attributable to the mesh and having a change in the cavity area. The vertical dashed lines delineate the frequency region of interest. The trend in spectral energy matches standard empirical trend lines in spectral energy for each region of the boundary layer [4]. Spectral energy is higher in the outer and transition region while it decreases towards the wall where the higher frequency fluctuations are generated. For all of the cavities, reductions in the energy spectra were generally seen at frequencies above 1.5 kHz or normalized at values of 0.75 in figs. 4 and 5.

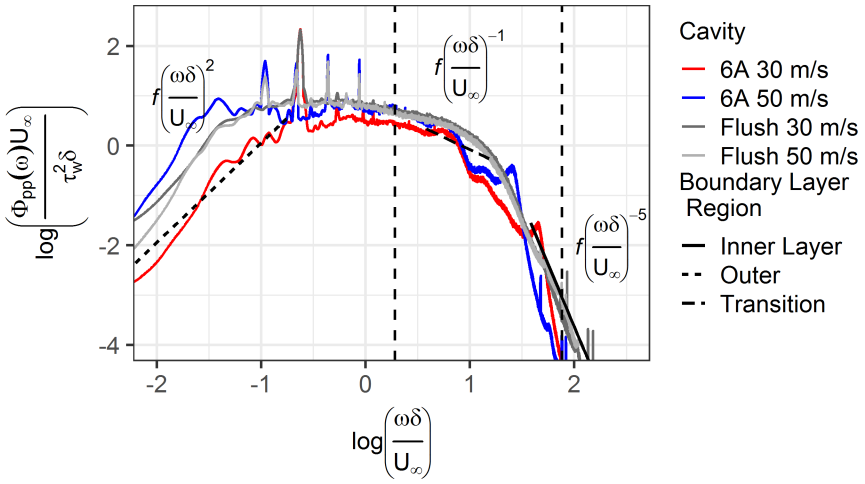

Fig. 4 Cavity 6A, no mesh and no change in area, acoustic spectra normalized with the boundary layer properties

B. Statistical Modeling

Initially the spectral energy data were fit to a generalized linear mixed effect model [21]. Equation 5 represents a generalized linear mixed effects model.

$$\boldsymbol{y} = \boldsymbol{X\beta} + \boldsymbol{Zb} + \boldsymbol{\epsilon} \tag{5}$$

In this equation $\boldsymbol{y}$ is a 1-D vector of response variable, the vector length, n is the number of experimental observations. $\boldsymbol{X}$ is a nxm design matrix where m is the number of model terms, the experimental factors of interest. $\boldsymbol{\beta}$ is a 1-D vector of length m of the model coefficients. $\boldsymbol{Z}$ is the design matrix of random observations or known sources of error, it has dimensions nxp, where p are the number of random observations. $\boldsymbol{b}$ is the length p vector of coefficients for the random observations. and $\boldsymbol{\epsilon}$ is the model error, a vector of length n. A mixed effects model was chosen because it allows for known sources of error to be accounted for in the model as random effects. For this experiment, the tunnel velocity was modeled as a random effect because the spectral energy levels increase with velocity which is a known

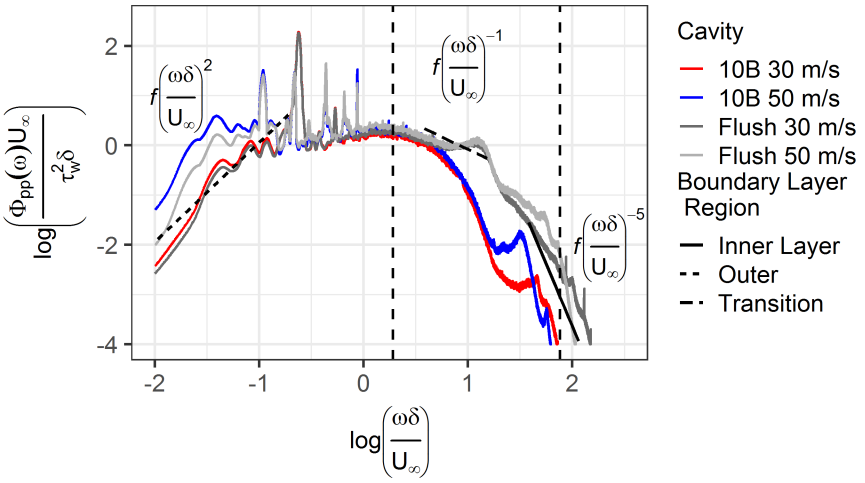

Fig. 5 Cavity 10B, mesh with change in area, acoustic spectra normalized with the boundary layer properties

effect. The microphone used for each measurement was also modeled as a random effect in case it could be shown that a microphone had a small bias. This concern was confirmed in the resulting analysis which showed that spectral energy was offset depending on which microphone was used as shown in fig. 6. This bias was only detectable due to randomizing runs and randomizing which microphones were used with which cavity between runs. The microphones

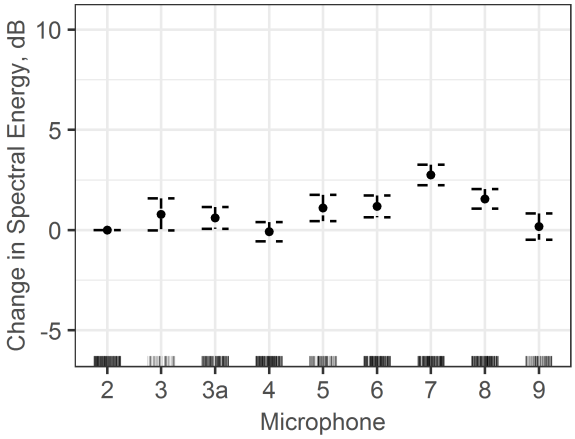

Fig. 6 Effect of microphone measurement bias with 95% confidence intervals

should be statistically indistinguishable from each other, however microphone 7 is shown to have a 2.5 dB bias compared to the other microphones. By accounting for this random effect in a mixed model, the measurement error in the response variables due to the microphones is accounted for and does not influence the results by biasing the data towards measurements made with a specific microphone.

Initially, this analysis was performed with a linear model. The response variables were determined by integrating the overall spectral energy over the frequency range of interest. While this initial model showed that parameters such as depth, mesh, and chamfer were significant, it didn't capture the nonlinear dependence with frequency. Figures 4 and 5, show the presence of this relationship between frequency and spectral energy and thus the need to take it into account. This was done by calculating the spectral energy for all third octave bands up until the 6.3 kHz band. This approach captures the frequency dependency while reducing the computational demands of the analysis. Since the relationship between the response variables and frequency is not linear, a linear model is unsuitable if we wish to evaluate how the effect of different experimental factors changes with frequency. This is shown by figure 7a, which shows the heteroskedasticity of the linear model as described by eq. 5. Heteroskedasticity is when the variance of residuals does not have a constant distribution. Therefore a generalized additive model (GAM) was chosen to model the

dataset. GAM's are extensions of linear models and conceptually similar. The primary difference is that instead of linear terms, GAMs allow for the experimental factors x_n, from the vector $\boldsymbol{X}$, to be modeled with smooth splines [22]. Notionally, the coefficients in a linear model are replaced by smooth splines as shown in equation 6, where $f(x_{nm})$ are splines that replace the coefficients in $\boldsymbol{\beta}$, and β_0 is the model intercept, a vector of length m.

$$y_n = \boldsymbol{\beta_0} + f_1(x_{n1}) + f_2(x_{n2}) + \ldots + f_m(x_{nm}) + \epsilon_n \tag{6}$$

Each spline term is the estimate of the contribution of each experimental factor to the overall response variable. These terms are additive and when combined result in the estimate of the response variable. These splines can be individual factors or combinations of factors, known as interaction terms. GAM's also mixed effect modeling. Figure 7b shows the improvement over linear models. The curve in the mean residual distribution is now much closer to the ideal zero mean line which is known as homoskedasticity. Additionally, the magnitude of residuals is also smaller, implying a better fit of the data. GAM's were fit to the spectral energy response variables datasets using the *mgcv R* package.

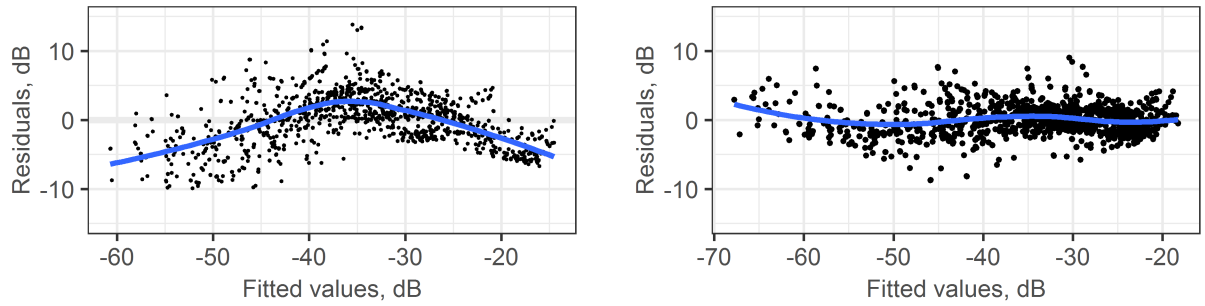

(a) Linear Residual Distribution **(b) GAM Residual Distribution**

Fig. 7 Comparison of the effect of model selection on residual distribution

1. Turbulent Boundary Layer Spectra

A generalized additive model was fit to examine the relationship between the wall pressure spectra of the boundary layer and the experimental factors. The resulting model thus incorporates the cavity geometric parameters and the free stream velocity. Since the boundary layer spectral energy decays with frequency[13] as discussed previously and shown in fig 5 it is important to include the nonlinear effect of frequency in the model, necessitating the use of a GAM. This model was fit over third octave bands covering frequencies from 250 Hz to 6.3 kHz, the total energy within each band was calculated in terms of decibels. The trend of spectral energy with frequency is of primary interest and not the fluctuations at each discrete frequency. Therefore third octave bands are advantageous as the spectral fluctuations within each band are integrated into the total amount of energy per band, smoothing out the response variable.

The primary constraint while developing this model was to maintain a connection between the physical significance of model terms and the response variable in order to support future validation of analytical models, CFD simulations, and experiments. This means, that terms for the effect of the experimental factors were only included if a physical explanation can be attributed to them. This approach avoids over-fitting the model by including every possible model term. Since it is known a priori that the spectra will vary with frequency, free-stream velocity, and that the microphone used, these terms were chosen as the initial model terms. Once this preliminary model showed that these assumptions were valid, geometric terms were added iteratively. In GAM modeling, terms can be added as linear terms or as spline basis functions that incorporate the non-linear relationship between the response variable and the experimental factor. Once the effect of each factor, the main effects, were incorporated into the model, the next step was to determine if their were any interactions between factors. Being able to evaluate interactions is an important benefit that results from applying DOE to the initial experimental design [12, 15]. After each iteration the updated model was evaluated in terms of the goodness of fit and more importantly the suitability of the model terms. Goodness of fit was evaluated in terms of the Akaike information criterion (AIC), the percent of deviance explained by the model, and the residuals. AIC is a standard metric which combines an expression for the goodness of fit with the number of parameters used to fit the model [14]. Therefore the best model is the one that has the best fit to the data with the fewest model terms. A

Table 4 Cavity spectral energy statistical model diagnostics

	Random Effects Only	Final Model
AIC	7550.14	5666.43
BIC	7653.07	5884.40
Log Likelihood	−3755.04	−2790.80
Deviance	28605.94	6190.86
Deviance explained	0.81	0.96
Dispersion	23.04	5.07
R^2	0.80	0.96
GCV score	3794.75	2878.85
Num. obs.	1260	1260
Num. smooth terms	3	7

lower AIC is better but this term can only be used to compare models based on the same dataset. Residuals should be normally distributed and as close to zero as possible [22]. Large residuals or residuals that exhibit heteroskedasticity indicate that the model is missing a term that explains a non-linearity or a source of variance.

Table 4 compares the initial random effects only model which only includes frequency, microphones, and free-stream velocity with the final model that includes the geometric parameters. The final model has a reduced AIC, deviance, and the R^2 value increased from 80% to 96%. Figure 8 shows the residual diagnostic plots. The histogram in fig. 8b shows that the residuals are close to zero and indicates that they are normally distributed. This is further supported by the quantile-quantile plot, fig. 8a, which plots the probability distribution of the model residuals against a normal distribution. Since the residuals are close to the line, this supports the assumption that the residuals are normally distributed [22]. Figure 8c shows that the model residuals are homoscedastic as they are closely distributed around zero, indicating that there are no non-linear effects remaining unincorporated into the model. Figure 8d compares the experimental data with the model prediction. As shown, these points are closely distributed around a slope of one, indicating that the model adequately represents the data.

In conjunction with evaluating each model as a whole compared to the random effects only model, each model term was evaluated for the size of its effect on the response variable and its statistical significance. Statistical significance was determined by p-values less that 0.05, which is the probability that change in variance or effect size is falsely attributed to that model term. Finally, it is critical that a physical interpretation of the model term exists. For example, both the cavity depth and presence of a mesh covering have physical interpretations. It is assumed that a mesh can be modeled by imposing an impedance across a cavity opening. As discussed previously, eq. 1 from duct acoustics suggests that cavity depth can be explained by cut-off modes decaying exponentially with distance [11]. This exponential relationship for depth was linearized by taking the natural log in order to better model this term.

The measured effect on spectral energy for each of the model terms is listed in table 5. These experimental factors included as model terms are statistically significant as shown by their p-values. The effect size is the linear coefficient of the model. The overall change in spectral energy due to each term is this effect size multiplied by experimental factor. For example, for a cavity that has a depth of 10 mm, the overall effect is $log(10) \cdot (-0.65) = -1.5$ dB. Both the aperture area and change in area have effect sizes of zero. This is because the effect of these model parameters are included in the spline basis functions listed in table 6 as well as the interaction terms. The presence of a mesh reduces the spectral energy by approximately 8 dB when the linear and non-linear terms are combined. There are two interaction terms of interest, the effect of increasing area and reduction in area are significantly affected by the presence of the mesh. When a mesh is present, a larger cavity opening reduces the measured spectral energy. It is important to note that the effect size of −0.03 appears small but wasn't rejected in accordance with the previously described methodology. This is because the area terms are on the order of 100 mm^2 which therefore results in a total reduction around 3 dB when a mesh is present. The other interaction term has the opposite effect which suggests that the more you reduce the area without a mesh, the more spectral energy is reduced. With a mesh, this no longer has the same effect. It is important to note that the model terms are additive which means that despite the spectral energy increasing with decreasing area for a

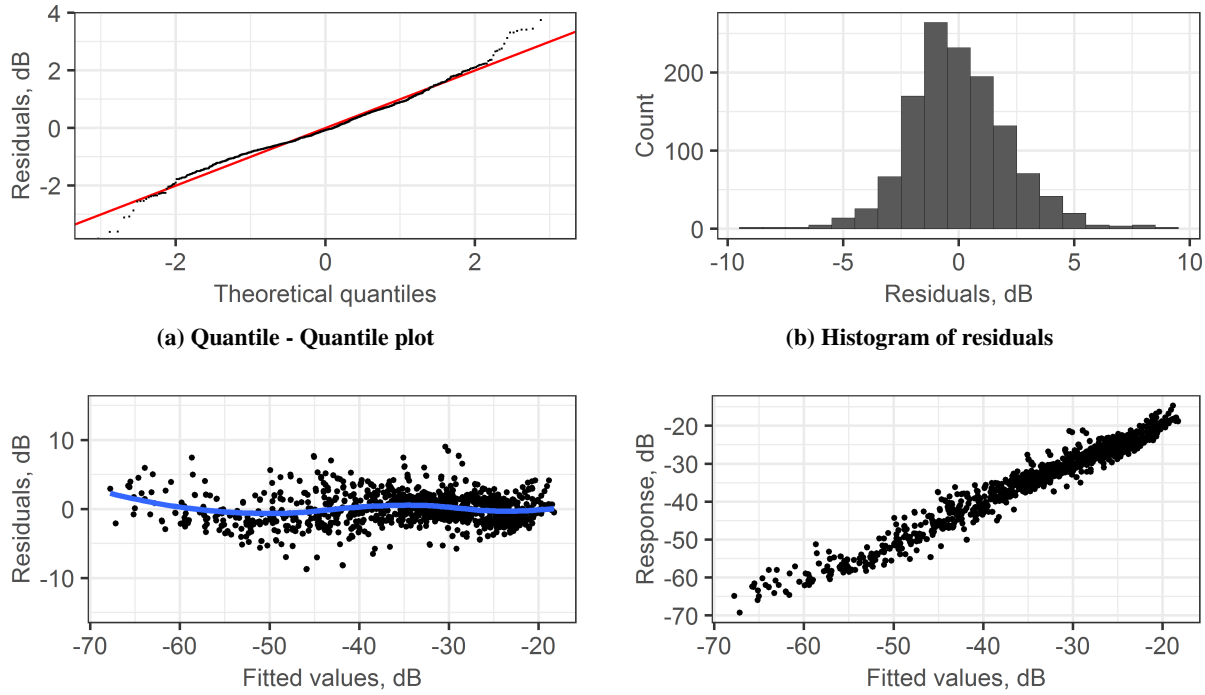

(a) Quantile - Quantile plot

(b) Histogram of residuals

(c) Homoscedasticity of residuals

(d) Model response vs. experimental values

Fig. 8 Boundary layer spectral energy GAM model residual diagnostic plots

mesh, the presence of the mesh reduces the total spectral energy.

Table 6 lists the spline basis functions and their estimated degrees of freedom. EDF's should be lower than the number of degrees of freedom for each variable. This table shows that the variance in spectral energy due to changing frequency is statistically significant, which is expected. The effect of the mesh, in addition to have a linear offset as discussed previously also varies with frequency. This is the case for the cavity aperture area and change in area as well. These basis functions are best interpreted visually. Figure 9 highlights the variance in spectral energy with frequency. The effect size should be interpreted as relative to the model mean also known as the intercept of −52 dB. The variation with frequency is the dominant term in the model as shown in fig. 9a, the spectral energy varies by as much as 30 dB over the frequency range of interest. Another important random effect is the free-stream tunnel velocity. The overall estimate of the influence of velocity is shown in fig. 9b. This plot shows the cumulative effect of velocity and frequency and includes the model estimate term which results in the overall model prediction. Spectral energy increases by approximately 10 dB for the higher velocity. Figure 10a shows that the effect of mesh varies with frequency. According to the model, the mesh has a linear reduction in spectral energy until 2 kHz. Given that for most materials impedance often is frequency dependent, this result is expected. However, additional experiments may be required to determine how the different geometric parameters of the mesh such as the thread diameter and density influence this relationship.

Figures 11 - 13 provide a visualization of the model predictions. These plots show how depth, aperture area, and change in area affect the spectral energy as well as the interaction between area and change in area with the presence of a mesh covering. Figure 11 shows that as the cavity area decreases from the cavity aperture, the spectral energy is reduced, especially at higher frequencies. This effect is possibly due to the same principle in duct acoustics for which changes in area cause a reflection in the pressure waves [11], potentially reducing the overall energy. This effect becomes apparent above 2.5 kHz. A sample of the measured data is plotted on top of the model and shows that the model does a reasonable job of matching predictions with measurements. The interaction between changing the cavity area and the presence is clearly shown. When there is no mesh, the changing area has a more pronounced effect. This is in contrast to when there is a mesh, where the effect of the area reduction is much less pronounced and only the largest reduction is statistically distinct from the other geometries. It is possible that when the mesh reduces the energy in the boundary layer that the effect of changing area is less effective. Figure 12 shows the reduction in spectral energy with depth.

Table 5 Cavity spectral energy linear terms statistical model summary

	Estimated Effect Size (Standard Error)
(Intercept)	−52.16 (0.43)***
log(Depth)	−0.65 (0.07)***
Area	0.00 (0.00)
Change in Area	0.00 (0.00)
Mesh Yes	−2.96 (0.34)***
Area:Mesh Yes	−0.03 (0.01)***
Change in Area:Mesh Yes	−0.96 (0.12)***

$^{***}p < 0.001$, $^{**}p < 0.01$, $^{*}p < 0.05$

Table 6 Cavity spectral energy basis functions statistical model summary

	Effective Degrees of Freedom (EDF) (Standard Error)
EDF: s(Center Freq)	5.49 (6.30)***
EDF: s(Microphone)	7.47 (8.00)***
EDF: s(Center Freq):Mesh No	1.02 (1.03)
EDF: s(Center Freq):Mesh Yes	3.17 (4.05)***
EDF: s(Center Freq):Actual Speed	6.19 (7.02)***
EDF: s(Center Freq):Change Area	5.19 (6.08)***
EDF: s(Center Freq):Area	6.51 (7.45)***

$^{***}p < 0.001$, $^{**}p < 0.01$, $^{*}p < 0.05$

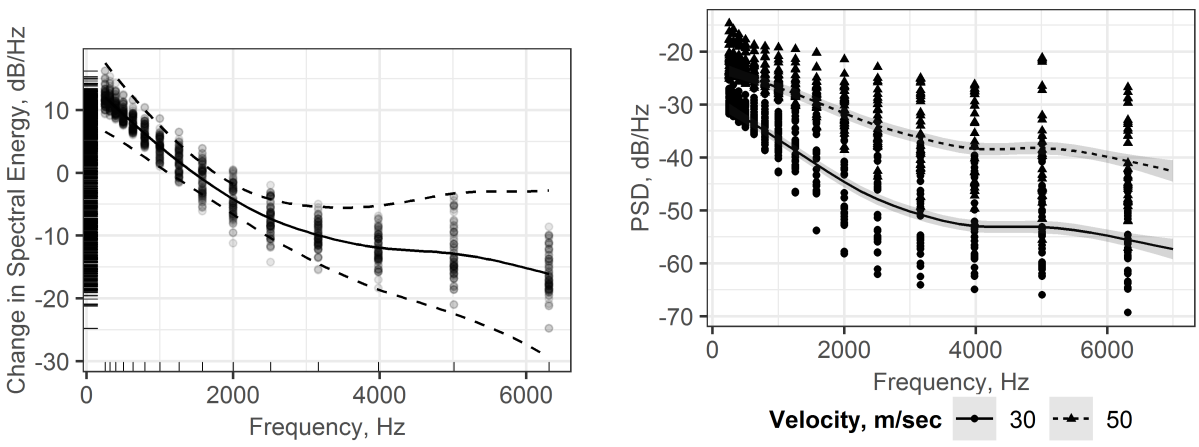

(a) Estimated change in spectral energy with frequency

(b) Comparison of spectral energy at two velocities.

Fig. 9 Change in spectral energy due to random effects

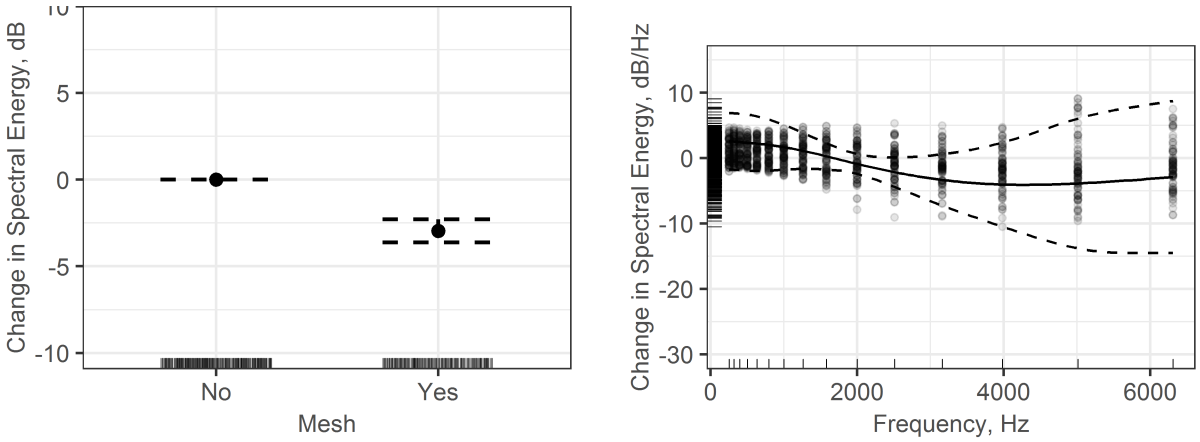

(a) Effect size of mesh linear term **(b) Change of mesh effect size with frequency**

Fig. 10 Mesh effect on boundary layer spectral energy

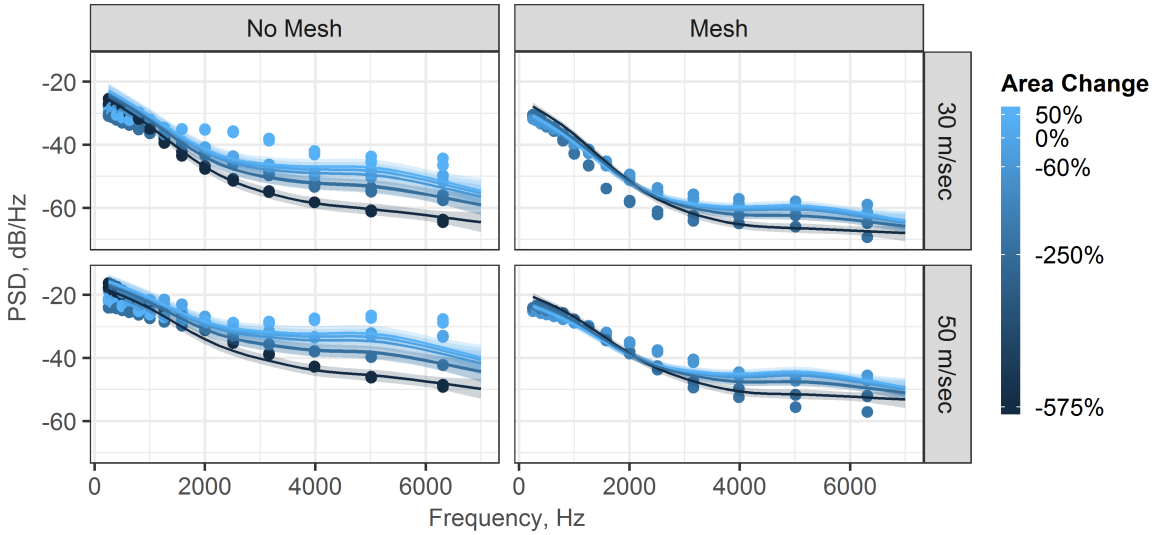

Fig. 11 Effect of changing cavity area with depth on boundary layer spectra

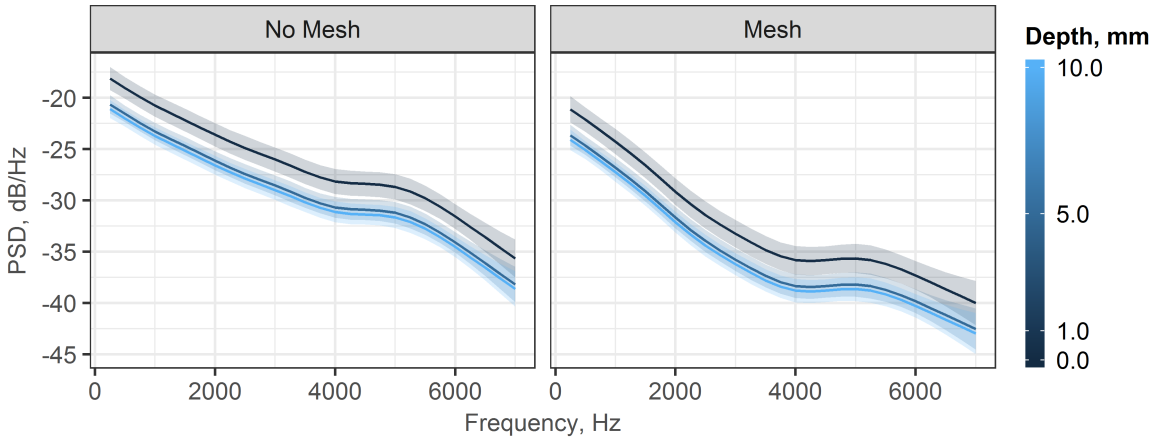

Fig. 12 Effect of increasing depth on boundary layer spectra

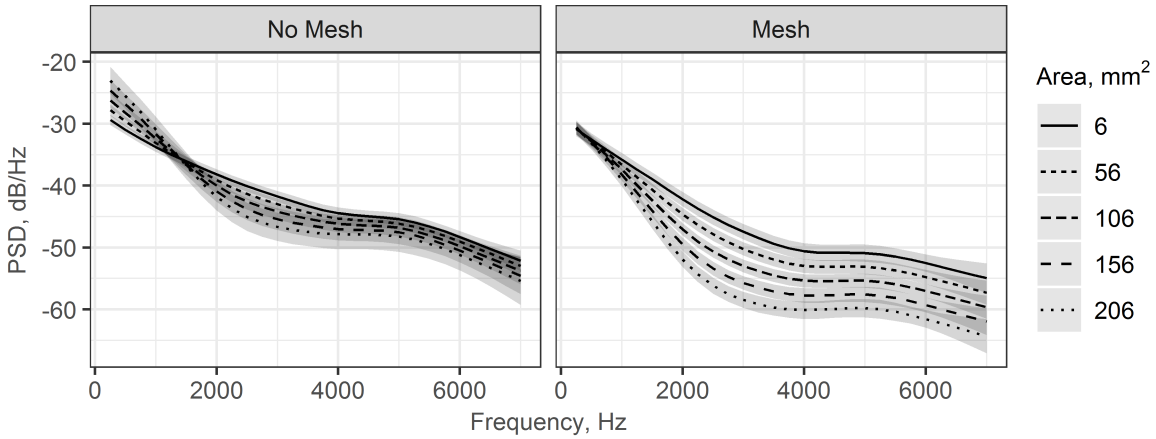

Fig. 13 Effect of interaction between cavity opening area and mesh on boundary layer spectra

The model suggests that increasing depth has an exponential effect on the overall spectral energy. It is predicted that increasing the depth becomes less effective the deeper the cavity. This is supported in the equations for duct acoustics in which cut-off modes decay exponentially, therefore after a certain depth, the cavity does not continue to be as effective at reducing the boundary layer spectral energy. This figure also indicates that the mesh reduces the spectral energy for all depths equally with no interaction. Finally fig. 13 shows the effect of the cavity's aperture area has on the spectral energy. It is clear that without the mesh, the size of the cavity aperture area, at least for this experiment, has minimal effect. The model suggests that at lower frequencies, the larger cavities result in more energy from the boundary layer being propagated to the microphone. However, these estimates' confidence intervals overlap significantly. The presence of the mesh has the opposite influence. The spectral energy clearly decreases with increasing area if there is a mesh. One possible explanation is that the mesh reduces the boundary layer pressure fluctuations sufficiently [5] such that the remaining energy is better dissipated with a larger area. It is important to note that these predictions were plotted holding everything but the frequency, area, and mesh constant.

V. Conclusion

This study evaluated how different cavity geometries affect acoustic measurements when a microphone is mounted in the base of a cavity. A systematic DOE approach quantified the effect individual parameters including depth, diameter, mesh, and change in area have on the reduction in turbulent boundary layer spectral energy. This approach provides a statistically rigorous organizational framework for the experiment and follow on analysis. A generalized additive model modeled the size of the effect cavity geometries have with respect to the two response variables. GAM's provide insight into the nonlinear relationship between cavity geometries and the response variables over the frequency range of interest. This modeling approach was well suited for the boundary layer spectra and showed that the mesh reduces the spectral energy by 8 dB when the linear and non-linear terms are combined. It also showed that energy decreases exponentially with increasing depth. Finally it quantified the relationship between the amount of reduction in cavity area and the presence of a mesh. These effects are not just stochastic relationships, the propagation of pressure waves within an infinite duct provides a physical explanation that supports the statistical model.

The experimental results and the explanatory stochastic model are initial steps in developing an analytical framework for designing microphone cavities to enable improved aeroacoustic measurements. These data will be used to validate deterministic models that use methods for solving the wave equation in a duct to the constraints of a cavity. Additionally these data will support the development of models that use finite element methods and a lattice Boltzmann computational fluid dynamics simulations to analyze cavity designs.

References

[1] Sijtsma, P., "Phased array beamforming applied to wind tunnel and fly-over tests," Report NLR-TP-2010-549, National Aerospace Laboratory NLR, December 2010.

[2] Merino Martinez, R., "Microphone arrays for imaging of aerospace noise sources," Thesis, 2018. doi:a3231ea9-1380-44f4-9a93-dbbd9a26f1d6.

[3] Howe, M. S., "Surface pressures and sound produced by turbulent flow over smooth and rough walls," *The Journal of the Acoustical Society of America*, Vol. 90, No. 2, 1991, pp. 1041–1047. doi:10.1121/1.402292.

[4] Blake, W. K., *Mechanics of Flow-Induced Sound and Vibration*, second edition. ed., Academic Press, an imprint of Elsevier, London, 2017.

[5] Jaeger, S., Horne, W., and Allen, C., "Effect of surface treatment on array microphone self-noise," *6th Aeroacoustics Conference and Exhibit*, American Institute of Aeronautics and Astronautics, 2000. doi:10.2514/6.2000-1937.

[6] Kamruzzaman, M., Lutz, T., Würz, W., Shen, W. Z., Zhu, W. J., Hansen, M. O. L., Bertagnolio, F., and Madsen, H. A., "Validations and improvements of airfoil trailing-edge noise prediction models using detailed experimental data," *Wind Energy*, Vol. 15, No. 1, 2012, pp. 45–61. doi:10.1002/we.505, URL https://doi.org/10.1002/we.505.

[7] Oerlemans, S., Fisher, M., Maeder, T., and Kögler, K., "Reduction of Wind Turbine Noise Using Optimized Airfoils and Trailing-Edge Serrations," *AIAA Journal*, Vol. 47, No. 6, 2009, pp. 1470–1481. doi:10.2514/1.38888, URL https://doi.org/10.2514/1.38888.

[8] Sijtsma, P., "CLEAN Based on Spatial Source Coherence," *International Journal of Aeroacoustics*, Vol. 6, No. 4, 2007, pp. 357–374. doi:10.1260/147547207783359459.

[9] Horne, W., and James, K., *Concepts for reducing the self-noise of in-flow acoustic sensors and arrays*, Aeroacoustics Conferences, American Institute of Aeronautics and Astronautics, 1999. doi:doi:10.2514/6.1999-181510.2514/6.1999-1815, URL https://doi.org/10.2514/6.1999-1815.

[10] Fleury, V., Coste, L., Davy, R., Mignosi, A., Cariou, C., and Prosper, J. M., "Optimization of Microphone Array Wall Mountings in Closed-Section Wind Tunnels," *AIAA Journal*, Vol. 50, No. 11, 2012, pp. 2325–2335. doi:10.2514/1.J051336, URL https://doi.org/10.2514/1.J051336.

[11] Rienstra, A., S.W.; Hirschberg, *Fundamentals of Duct Acoustics*, Eindhoven University of Tecnology, 2018. URL http://www.win.tue.nl/~sjoerdr/papers/VKI_Rienstra.pdf.

[12] DeLoach, R., *Analysis of Variance in the Modern Design of Experiments*, Aerospace Sciences Meetings, American Institute of Aeronautics and Astronautics, 2010. doi:doi:10.2514/6.2010-111110.2514/6.2010-1111, URL https://doi.org/10.2514/6.2010-1111.

[13] Goody, M., "Empirical Spectral Model of Surface Pressure Fluctuations," *AIAA Journal*, Vol. 42, No. 9, 2004, pp. 1788–1794. doi:10.2514/1.9433, URL https://doi.org/10.2514/1.9433.

[14] Montgomery, D. C., *Design and analysis of experiments*, eighth edition. ed., John Wiley & Sons, Inc., Hoboken, NJ, 2013.

[15] Landman, D., Simpson, J., Mariani, R., Ortiz, F., and Britcher, C., "Hybrid Design for Aircraft Wind-Tunnel Testing Using Response Surface Methodologies," *Journal of Aircraft*, Vol. 44, No. 4, 2007, pp. 1214–1221. doi:10.2514/1.25914.

[16] Morgan-Wall, T., and Khoury, G., *skpr: Design of Experiments Suite: Generate and Evaluate Optimal Designs*, 2018. URL https://CRAN.R-project.org/package=skpr, r package version 0.47.5.

[17] Jong, A. T. D., "Aeroacoustic Resonance of Slender Cavities: An Experimental and Numerical Investigation," Thesis, 2012.

[18] Arguillat, B., Ricot, D., Robert, G., and Bailly, C., "Measurements of the wavenumber-frequency spectrum of wall pressure fluctuations under turbulent flows," *11th AIAA/CEAS Aeroacoustics Conference*, American Institute of Aeronautics and Astronautics, 2005. doi:doi:10.2514/6.2005-28555.

[19] Bruun, H., *Hot-wire Anemometry: Principles and Signal Analysis*, Oxford University Press, 1995. URL https://books.google.nl/books?id=PkAnIqXGkY0C.

[20] Nieuwstadt, F. T. M., Westerweel, J., and Boersma, B. J., *Turbulence: Introduction to Theory and Applications of Turbulent Flows*, 1st ed., Springer International Publishing, 2016. doi:10.1007/978-3-319-31599-7.

[21] Bates, D., Mächler, M., Bolker, B., and Walker, S., "Fitting Linear Mixed-Effects Models Using lme4," *Journal of Statistical Software*, Vol. 67, No. 1, 2015, pp. 1–48. doi:10.18637/jss.v067.i01.

[22] Wood, S. N. W. S. N., *Generalized additive models : an introduction with R*, CRC Press, Boca Raton, Florida, 2017.